Identification and characterization of key haem pathway genes associated with the synthesis of porphyrin in Pacific oyster (*Crassostrea gigas*)

Biyang Hu [a], Qi Li [a,b,*], Hong Yu [a], Shaojun Du [c]

[a] *Key Laboratory of Mariculture, Ministry of Education, Ocean University of China, Qingdao 266003, China*
[b] *Laboratory for Marine Fisheries Science and Food Production Processes, Qingdao National Laboratory for Marine Science and Technology, Qingdao 266237, China*
[c] *Institute of Marine and Environmental Technology, Department of Biochemistry and Molecular Biology, University of Maryland School of Medicine, Baltimore, MD, United States*

ARTICLE INFO

ABSTRACT

Molluscs exhibit diverse shell colors. The molecular regulation of shell coloration is however not well understood. To investigate the connection of shell coloration with pigment synthesis, we analyzed the distribution of porphyrins, a widespread group of pigments in nature, in four Pacific oyster strains of different shell colors including black, orange, golden, and white. The porphyrin distribution was analyzed in oyster mantles and shells by fluorescence imaging and UV spectrophotometer. The results showed that red fluorescence emitted by porphyrins under the UV light was detected only on the nacre of the orange-shell strain and mantles of orange, black and white-shell strains. Extracts from newly deposit shell, nacre and mantle tissue from orange-shell specimens showed peaks in UV–vis spectra that are characteristic of porphyrins, but these were not observed for the other shell-color strains. In addition, genes of the haem synthetic pathway were isolated and characterized. Phylogenetic analysis of *CgALAS*, *CgALAD*, *CgPBGD*, *CgUROS*, and *CgUROD* provide further evidence for a conserved genetic pathway of haem synthesis during evolution. Differential expression of the haem genes expressed in mantle tissues support these findings and are consistent with porphyrins being produced by the orange strain only. Tissue *in situ* hybridization demonstrated the expression of these candidate genes at the outer fold of *C. gigas* mantles where shell is deposited. Our studies provide a better understanding of shell pigmentation in *C. gigas* and candidate genes for future mechanistic analysis of shell color formation in molluscs.

1. Introduction

It has been well documented that diverse appearance of colors and patterns play important roles in many aspects of animal life and adaptation, such as social signaling, antipredator defenses, parasitic exploitation, thermoregulation, and protection from ultraviolet light, microbes, and abrasion (Cuthill et al., 2017). Mollusca with their colorful shells provide valuable experimental subjects to investigate the cellular and molecular mechanisms of shell color formation (Frederic et al., 2012). The molluscs shell forms at the interface of animal and environment. The formation of shells involves controlled deposition of calcium carbonate within a framework of macromolecule matrix (Kocot et al., 2016). The shell color is determined by pigments deposit by the

mantle (Taylor et al., 1969).

The molecular pathways of pigmentation have been characterized in plants, insects, and bony fish (Grotewold, 2006; Joron et al., 2006; Braasch et al., 2007; Wittkopp and Beldade, 2009). Transcriptomic, proteomic, and genomic data in relation to the mollusc shell formation and pigmentation has been generated in molluscs (*e.g.*, pearl mussel, scallop, pacific oyster, hard clam, and pearl oysters)(Bai et al., 2013; Ding et al., 2015; Feng et al., 2015; Hu et al., 2019; Xu et al., 2019; McDougall and Degnan, 2018). Specific genes related in shell color formation has only been studied in a few mollusc species, such as marine snails, Pacific oyster, and black-lipped pearl oyster (Lemer et al., 2015; Feng et al., 2017; Williams et al., 2017; Feng et al., 2018). Genes in the haem synthetic pathway have been implicated in shell pigments of

Clanculus margaritarius and *C. pharaonius* (Williams et al., 2017). The shell color in black-lipped pearl oyster was shown to be influenced by genes involved in the biomineralization of the calcareous layer (Lemer et al., 2015). And genes associated with production of porphyrin pigments in tissues were identified in *Clanculus* species (Williams et al., 2017). In addition to pigmentation, several conserved proteins have been implicated in shell formation in *C. gigas* and other molluscs (Feng et al., 2017). Moreover, several lncRNA and mRNA transcripts associated with shell pigmentation have been identified that influence pigment biosynthesis including melanin, carotenoid and tetrapyrrole (Feng et al., 2018). However, little is known on the molecular pathway of shell pigmentation in molluscs (Mann and Jackson, 2014).

Pigments including melanin, porphyrin are believed to contribute to shell colors in molluscs (Comfort, 1949; Comfort, 1950d; Comfort, 1950a; Comfort, 1950b;). Porphyrins are a widespread group of pigments in nature. They include chlorophyll for photosynthesis in plants and hemoglobin for oxygen transportation in blood of vertebrates (Negro et al., 2009). Porphyrins emit red fluorescence when illuminated by ultra violet (UV) light (With, 1978). The biochemical pathways involved in porphyrin production are known. The production of uroporphyrin I and III is derived from the oxidation of uroporphyrinogen I and III which belongs to non-enzymatic side paths. Uroporphyrin I and III are found in molluscs (Nicholas and Comfort, 1949; Comfort, 1950c; Williams et al., 2016; Bonnard et al., 2020). Previous studies in purple-shell oysters revealed the presence of uroporphyrin in shell and mantle, indicating that porphyrins may derive from the non-enzymatic oxidation of uroporphyrinogen I and III associated with cellular respiration in the mantle of *Crassostrea gigas* (Bonnard et al., 2020). Genes associated with porphyrin metabolism pathway have been identified in marine snails (Williams et al., 2017). In addition, a recent study indicated that 5-Aminolaevulinate synthase (ALAS) in Yesso scallop showed significantly higher levels of expression in mantle tissue producing brown shells than mantle producing white shells (Mao et al., 2020). These studies provide candidate genes for porphyrin shell coloration in molluscs.

Pacific oyster *C. gigas* is a widely distributed and economically important species in the world. It has become a potential model for molluscs research (Yu et al., 2016). Strains of different shell colors have been identified and established in Pacific oysters. To assess the contribution of porphyrins on shell color formation, we analyzed porphyrin contents in shells and mantles of four oyster strains of different colors using fluorescent microscopy and UV spectrophotometry. The data showed that red fluorescence emitted by porphyrins under UV light was observed only on the nacre of orange-shell strain and mantles of orange-shell, black-shell and white-shell strains. Porphyrins features characteristic peaks for in their UV–visible absorption spectra: the maximum absorption wavelength of porphyrins is about 400 nm, known as the Soret band (Wijesekera and Dolphin, 1985), and there are four weaker absorption wavelength called Q-bands in metal-free porphyrins (Dixon, 2000). Analysis of extracts from newly deposit shells and mantles showed the characteristic peaks of porphyrins in the orange-shell strain. However, the characteristic peaks of porphyrins were undetectable in other shell-color strains. Given that uroporphyrin I and III are the side products of the haem pathway, we cloned five genes in the haem pathway that include ALAS, ALAD, PBGD, UROS, and UROD (*CgALAS, CgALAD, CgPBGD, CgUROS,* and *CgUROD*). Bioinformatics and expression analyses revealed that shell porphyrins are synthesized *de novo* by the *C. gigas*. Several conserved domains were detected in the predicted protein sequences of *CgALAS, CgALAD, CgPBGD, CgUROS,* and *CgUROD*. Phylogenetic analysis of *CgALAS, CgALAD, CgPBGD, CgUROS,* and *CgUROD* provide evidence for a conserved genetic pathway of haem synthesis during evolution. Expression analysis by *in situ* hybridization showed the expression of candidate genes at the outer fold mantle. Significant difference in gene expression was detected in key haem synthetic pathway in mantle tissues of different shell color strains. Collectively, our work advances the understanding of shell color formation in molluscs, linking shell pigments with genetic pathway responsible for their biosynthesis. The high variability of gene expression in different shell colors provided the basis for future investigation the expression patterns of candidate genes with different shell colors in molluscs.

2. Materials and methods

2.1. Samples

Five lines of Pacific oysters named the whole white shell full-sib families (W), whole black shell full-sib families (B), whole golden shell full-sib families (G), whole orange shell full-sib families (O), and partially pigmentation shell full-sib families (N), were developed through six-generation successive family selective breeding. They exhibited stable hereditary shell color traits. The original parents of white, black, golden, orange and partially pigmented *C. gigas* were selected locally from cultured populations in Weihai, Shandong, China. The five kinds of *C. gigas* were collected in April 2019 (see Fig. 1 for photographic illustration of the shell phenotype of the different strains and Table S1 for list of specimens). Adult mantle was collected and frozen in liquid nitrogen and then stored at −80 °C until further processing. Samples stored in RNA store (Dongsheng Biotech, China) at −20 °C were used for RNA isolation. TRIzol reagent (Invitrogen, USA) was used to extract total RNA from *C. gigas* samples following the manufacturer's protocol. RNA concentration and purity were verified at optical density (OD)260/(OD)280 with NanoDrop 2000 (Thermo Scientific) spectrophotometer. PrimeScript™ Reverse Transcription Kit (Takara) was used to synthesize first-strand cDNA according to the manufacturer's instructions. The gDNA Eraser in PrimeScript RT reagent Kit was used to remove genomic DNA. The primers used for reverse transcription was RT Primer Mix which contained both Random 6 mers and Oligo dT Primer. Total RNA of each sample was diluted to same concentration for reverse transcription and the concentration of the cDNA products is 200 ng/μL.

2.2. Histological analysis and UV–visible spectrophotometry

The whole fresh mantle was cut from *C. gigas* after anesthetization in 20 g · L^{-1} MgCl$_2$ for 5 h. After cleaning the shell, the newly deposit shell was collected with tweezers and stored for the later application (see Supplementary Fig. S1 for detail about newly deposit shell). The cuticle and prismatic layer were removed by ultrasonic cleaner (PRIMA PM5–2000-TL) and sandpaper (Difeng) and was soaked in hypochlorous acid solution for 1 h to obtain the nacre layer. Five strains of *C. gigas* mantles and nacre layers were observed under fluorescent microscope (Olympus DP80) using both the white light and the UV light (Olympus, U-RFL-T), with the excitation wavelength at 330–400 nm and the emission wavelength at 425 nm, to detect the existence of porphyrins. The porphyrin pigments were extracted following methods of Williams (Williams et al., 2016). Pigments were extracted from the newly deposit shell, the nacre as well as the mantle of each strain by *ca.* 5 mL of 0.5 M Na-EDTA (pH 8) in a water bath for 1.5 h at 65 °C. The extracts were then centrifuged for 10 min at 300 ×*g* and their spectra absorption (300–800 nm with a resolution of 0.5 nm) were recorded using a Unico 2800 UV–visible spectrophotometer in 1 cm polystyrene cells against Na-EDTA solution as a blank. After the initial exposure to light for *ca.* 3 h, the solution was kept in darkness for 15 d and the spectra absorption was re-recorded to check the stability of the extracted pigments in the near-neutral Na-EDTA solution.

2.3. Identifying and cloning the coding-sequence of genes associated with pigment synthesis

The cDNA coding sequence of five genes in the haem pathway were amplified by PCR based on the sequence information download from the National Centre for Biotechnology Information (NCBI, http://www.

Fig. 1. Photographic illustration of the shell phenotype of the different strains of *Crassostrea gigas*.

ncbi.nlm.nih.gov; Accession: PRJEB35351; ALAS: LOC105330021; ALAD: LOC105330983; PBGD: LOC105326792 UROS: LOC105336067; UROD: LOC105347428). Specific primers (Table 1) were designed by the Primer Premier 6.0 software (Premier Biosoft International, Palo Alto, CA). The PCR was performed using 2× *Taq* Plus Master Mix (Dye Plus) (Vazyme biotech co., ltd.) with the following condition: pre-denaturation at 95°C for 3 min, 95°C for 15 s, Tm for 20 s, 72°C for 30-60 s, 35 cycles; 72°C for 5 min. The 10 μL PCR reaction contained 5 μL 2 × Taq Plus Master Mix II (Dye Plus), 0.4 μL of each primer(10μM) and 1 μL diluted cDNA (200 ng/μL). The PCR products were analyzed on a 1.5% agarose gel. The PCR products were purified using E.Z.N.A. Gel Extraction Kit (Omega BIO-TEK, China) and cloned into the TA/Blunt-Zero vector (Vazyme biotech co., ltd.). The DNA sequence was determined in both directions (PsnGene, China).

Table 1
A summary of primer sequences used in this study.

Primer name	Primer sequences	Experiment
CgALAS-F	5′-GTTGGTGATGCTGCCTTATGC-3′	Quantitative real-time PCR
CgALAS-R	5′-TCTGATGACTGAGGACACGAAG-3′	
CgALAD-F	5′-CAGCCTCCTCTCCCAGATCC-3′	
CgALAD-R	5′-CTGTCGCACGCATACTCTATCC-3′	
CgPBGD-F	5′-AACGCCTTCTACAGACACTACG-3′	
CgPBGD-R	5′-GAGGGAATGGGCAGAGAATAGG-3′	
CgUROS-F	5′-AGCCTGGATGGACACGAGAC-3′	
CgUROS-R	5′-CGCCGCCATTTCCTCACG-3′	
CgUROD-F	5′-GAGCGACTCACGGAACAGAAC-3′	
*Cg*UROD-R	5′-GACTTCCAACCAACCTCCTAGC-3′	
EF1-α-F	5′-AGTCACCAAGGCTGCACAGAAAG-3′	
EF1-α-R	5′-TCCGACGTATTTCTTTGCGATGT-3′	
CgALAS-RT-F	5′-TGTCTACTGCCTTGCGATGC-3′	Cloning
CgALAS-RT-R	5′-GGTTGCCTCCCTTTCTATTTCTG-3′	
CgALAD-RT-F	5′-CGCATGGTTCTATGATCGCTGAC-3′	
CgALAD-RT-R	5′-CTGTCCTGGTTCTCTGTCCTACG-3′	
CgPBGD-RT-F	5′-ATAGACATCGTCCCTATTCTGAAG-3′	
CgPBGD-RT-R	5′-GAGCCCTCCTTTATGTGAGTTAC-3′	
CgUROS-RT-F	5′-GCACGGATGGTAGAACTTGAG-3′	
CgUROS-RT-R	5′-GCGGTCTGGCTTTCGTATAG-3′	
CgUROD-RT-F	5′-TTCGCTTTACACTGTGATTTTGAG-3′	
CgUROD-RT-R	5′-CCACTATACAGCAATTCAGCATTC-3′	
CgALAS-ISH-F	5′-GGCTTCATCTTCACCACCAGTC-3′	*In situ hybridization*
CgALAS-ISH-R	5′-CACAGCACGGCGGTTATCAG-3′	
CgALAD-ISH-F	5′-AGCAGTGACCTATGCCAAAGC-3′	
CgALAD-ISH-R	5′-TGTCCTGGTTCTCTGTCCTACG-3′	
CgPBGD-ISH-F	5′-GTGTTGAATGCCGAGCAGACG-3′	
CgPBGD-ISH-R	5′-CGCCCTTGAGCCCTCCTTTATG-3′	
CgUROS-ISH-F	5′-ACAGTGAGCAGGCAAAGAACC-3′	
CgUROS-ISH-R	5′-TGCGGTCTGGCTTTCGTATAG-3′	
CgUROD-ISH-F	5′-GCTTCGCTGGTGCTCCTTG-3′	
CgUROD-ISH-R	5′-CACATTCTCAGGGTCGGTATCC-3′	

2.4. Molecular characteristic and phylogenetic analysis

The coding sequences of haem pathway genes were assembled using DNAMAN (Lynnon Biosoft) software and was used to predict the open reading frame. The isoelectric point (pI) and molecular weight (MW) of the deduced amino acid sequences were predicted using the Compute pI/MW Tool at the ExPASy site (https://web.expasy.org/protparam/). The TMHMM server v.2.0 (http://www.cbs.dtu.dk/services/TMHMM/) was used to predict transmembrane helices. The NetPhos server (http://www.cbs.dtu.dk/services/ NetPhos) was used to predict the phosphorylation sites. SMART (http://smart.embl-heidelberg.de/) was used to predict the conserved domain. The Jpred (http://www.compbio.dundee.ac.uk/jpred/) was used to predict the secondary structure. The signal peptide was analyzed by the SignalP4.1 (http://www.cbs.dtu.dk/services/SignalP/). The subcellular structure was predicted using the PSORT Prediction (http://psort1.hgc.jp/form.html). The protein sequences were aligned by ClustalW (Lynnon Biosoft, Los Angeles, CA) and modified by the ESPript 3.0 (Robert and Gouet, 2014). Phylogenetic trees were constructed by the maximum-likelihood (ML) method with 1000 bootstrap replicates using MEGA X software program. The accession numbers of full-length amino acid sequences of ALAS, ALAS1, ALAS2, ALAD, PBGD, UROS and UROD from different invertebrate and vertebrate species can be found in Supplementary Table S2. The sequences were aligned and modified by ClustalW (Lynnon Biosoft, Los Angeles, CA). The models used for the construction of the phylogenetic tree were chosen based on Bayesian Information Criterion value obtained by MEGA X software and were summarized in Supplementary Table S3.

2.5. Tissue in situ hybridization

Sense and antisense probes were synthesized using the DIG-RNA labeling Kit (Roche).

The target gene fragments were isolated by PCR with respective specific primers (Table 1). To generate sense and antisense probes, forward and reverse primers were tagged with a T7 promoter sequence, respectively. For the *in-situ* experiments, mantle tissues were fixed in a 4% paraformaldehyde phosphate buffered saline (pH 7.4) at 4 °C overnight and was dehydrated through a graded series of EtOH (from 50% to 100%). The transparent tissue was obtained by soaking in

absolute methanol for two times, then treated with methanol and xylene mixture (1:1) and infiltrated with absolute xylene twice. Xylene and paraffin mixture (1:1) was then used to infiltrate the tissue. Melted paraffin was used to embed the mantle tissue afterwards. Then 5-μm thick paraffin sections were prepared. ISH was carried out according to the published protocol with some modifications (Dos Reis et al., 2015). The sections were rehydrated through a graded series of EtOH into PBST (phosphate-buffered saline plus 0.1% Tween 20). Prior to pre-hybridization, all sections were digested with proteinase K (4 μg/mL) for 30 min at 37 °C. Prehybridization was carried out in hybridization buffer (5 SSC, 50% formamide, 100 μg/ml yeast t-RNA, 1.5% blocking reagent, 5 mM EDTA, 0.1% Tween-20) for 6 h at 65 °C. Then the sections were hybridized with 1 μg/mL sense or antisense probe overnight at 65 °C. Unbound probes were washed away, then antibody incubation was carried out with 1/5,000 anti-digoxigenin antibody (Roche) in blocking regents for 16 h at 4 °C. Samples were then washed several times in MABT (150mM sodium chloride, 100mM maleic acid, 0.1% Tween-20, pH 7.5), and in alkaline Tris buffer for 3 × 10 min. Color reactions were performed with 2% NBT/BCIP solution for 1 h in at room temperature or overnight at 4°C. After washing, eosin was used for counterstaining. Slides were dehydrated in graded alcohol solutions, air dried and mounted with neutral balsam. Specimens were photographed on a fluorescent microscope (Olympus BX53) with a digital camera (Olympus DP73).

2.6. Quantitative analysis of gene expression

Specific primers were designed to amplify five genes in the haem pathway using Primer 6 (Table 1). The reaction efficiency and R^2 of qPCR analysis were showed in Supplementary Table S5. A dissociation curve was generated in each case to check that only a single band was amplified. The qPCRs were performed in triplicate for each sample. Elongation factor 1-α (EF1-α) was used as an internal control. Quanti-Nova™ SYBR Green PCR Kit (Qiagen) was used to perform the quantitative analysis. 200 ng/μL cDNA products were used as templates for qRT-PCR. The 10 μL qRT-PCR reaction contained 5 μL 2× SYBR Green PCR Master Mix, 1.8 μL of each primer, and 1 μL diluted cDNA. The RT-qPCR amplification was conducted at 95 °C for 2 min, followed by 40 cycles at 95 °C for 5 s and 60 °C for 10 s. All data were given in the light of relative mRNA expression levels as means ± SE ($n = 3$), and were analyzed using the $2^{-\Delta\Delta CT}$ method (Livak and Schmittgen, 2001). Statistical analyses were performed using the GraphPad Software 8 with an independent *t*-test. Differences were deemed statistically significant at $p < 0.05$.

2.7. Western blot

Mantle tissues were collected from the five strains were firstly grounded in liquid nitrogen and proteins were extracted using cold PBS. The protein extracts were quantified using the commercial BCA protein assay kit (Servicebio, G2026). *CgALAS* protein were analyzed by western blotting using antibody against human ALAS (Beyotime AF1042) which shares 76% amino acid homologues with *CgALAS*. *CgPBGD* protein was analyzed using the antibody against rat (Beyotime AF2149) which shares 69% amino acid homologues with *CgPBGD*. Anti-beta Actin Mouse mAb (Servicebio GB12001) was used as the reference to control for the protein loading. Horseradish peroxidase (HRP)-conjugated anti-mouse IgG antibody (anti-mouse: 1:3000, Servicebio GB23301) was used as the secondary antibody. The AlphaEase FC Western blot analysis software was used to detect the immunoreactive band through enhanced chemiluminescence. Gray scale of the densitometry of the autoradiograph was used to quantify the detected *CgALAS* and *CgPBGD* protein content.

3. Results

3.1. Histological analysis and spectroscopy observation

The porphyrin pigments emit red fluorescence under the UV light. Fluorescence studies and UV–visible spectrometry had been proved to be informative methods for identifying uroporphyrin I and III (Williams et al., 2016). Thus, oyster mantles were examined under fluorescent microscopy to determine the existence of porphyrins. The data revealed a strong red fluorescence signal at the outer fold mantle of the orange-shell strain (Fig. 2), indicating the existence of porphyrins. In addition, a clear red fluorescence signal was also detected on the shell (Supplementary Fig. S2) and nacre (Fig. 3) of the orange-shell strain. Weaker red fluorescence was found in the black-shell and white-shell strain's outer fold of mantles (Fig. 4). There was no red fluorescence found in the golden-shell and normal-shell strains. Moreover, examination of Na-EDTA extracts from the shells and mantle of *C. gigas* show features characteristic for porphyrins in their UV–visible absorption spectra. The UV–visible absorption spectroscopy analysis revealed that the Na-EDTA extraction of orange-shell strain mantle and newly deposit shell showed typical feature of metal-free porphyrin: 400 nm Soret band and four Q bands (Fig. 5). The absorption wave of other strains showed no absorption peak. The Na-EDTA extraction of the orange-shell strain's mantle and the newly deposit shell stayed brown and stable in 15 days (Supplementary Fig. S3). The data indicate that metal free porphyrins were detected in the orange-shell strain of *C. gigas* but were undetectable in other strains. The fluorescence of different strains of *C. gigas* under UV light was summarized in Supplementary Table S4.

3.2. cDNA cloning and sequence analysis of key haem pathway genes

Genes in the haem synthetic pathway have been implicated in shell pigmentation of *C. margaritarius* and *C. pharaonius* (Williams et al., 2017). Gene transcripts of the haem synthesis enzymes were cloned from *C. gigas*. Expression analysis detected mRNA transcripts of several haem synthetic genes in *C. gigas* mantle tissue. These include aminole-vulinic acid synthase (ALAS), aminole-vulinic acid dehydratase (ALAD), porphobilinogen deaminase (PBGD), uroporphyrinogen-III synthase (UROS), uroporphyrinogen decarboxylase (UROD), coproporphyrinogen-III oxidase (CPOX), protoporphyrinogen oxidase (PPOX), and ferrochelatase (FECH). The first five genes in the pathway were believed to influence the synthesis of uroporphyrin I and uroporphyrin III. Five genes were successfully identified from the transcriptome database on NCBI's Sequence Read Archive (PRJNA381520/SUB2554964) following the strict screening step (Feng et al., 2018). The basic information of *CgALAS, CgALAD, CgPBGD, CgUROS, CgUROD* is summarized in Table 2.

The haem pathway is a well-known and highly conserved pathway which starts in the mitochondria. As succinyl-CoA is condensed to glycine to form aminolevulinic acid, in a reaction catalyzed by ALAS. The subcellular localization of these enzymes was predicted based on their protein sequences. As expected, *CgALAS* was predicted to be in the mitochondrial matrix space. *CgALAS* protein contained Preseq_ALAS, and Beta_elim_lyase conserved domains. *CgALAD*, *CgPBGD*, *CgUROS*, and *CgUROD* are predicted to be in the cytoplasm. ALA dehydratase condenses two molecules of ALA to form porphobilinogen (PBG) in the cytosol (Braz et al., 2001). The third enzyme PBGD condenses two molecules of porphobilinogen to form hydroxymethylbilane (HMB), which is highly unstable (Williams, 2017). *CgPBGD* protein contains the Porphobil_deam and Porphobil_deamC domain. UROS then converts HMB to uroporphyrinogen III (Ajioka et al., 2006). *CgUROS* protein has a HEM4 domain which functions during the second stage of tetrapyrrole biosynthesis. As for UROD, it is the fifth enzyme of the pathway which catalyzes the decarboxylation of uroporphyrinogen III to coproporphyrinogen III (Elder and Roberts, 1995). *CgUROD* protein contains a Pfam domain named URO-D domain. The last three steps of the
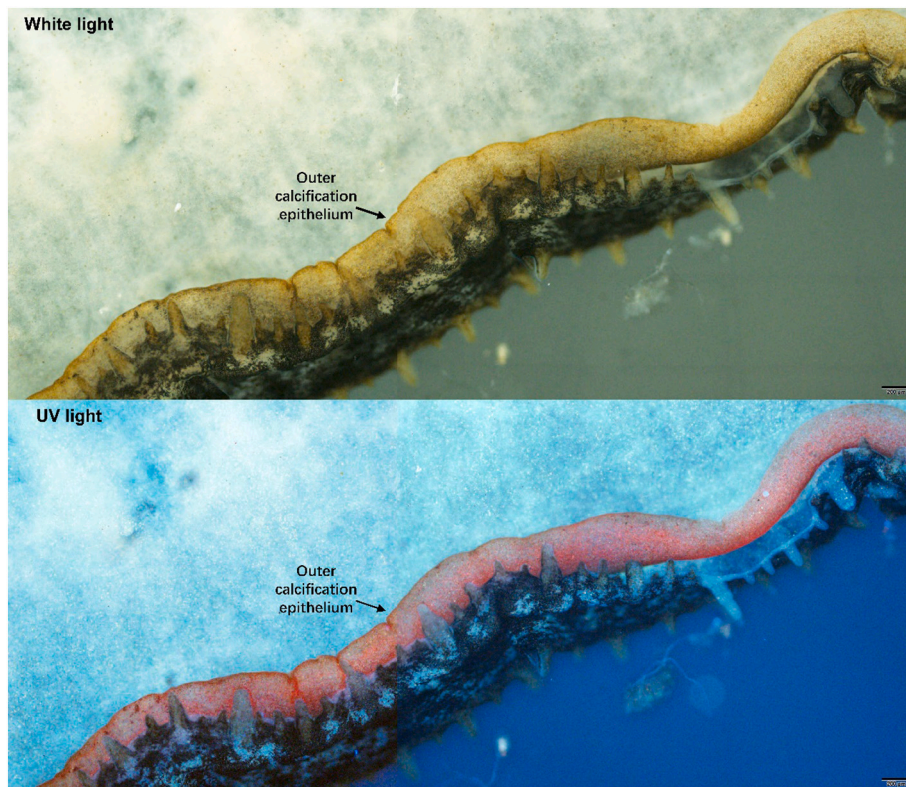
Fig. 2. The aragonite nacreous layer of *C. gigas* shells under white and ultraviolet (UV) light. Note that the nacre of the orange-shell strain fluoresces red under UV light. Other shell color strains' nacre does not have the red fluoresce under UV light. (For interpretation of the references to color in this figure legend, the reader is referred to the web version of this article.)
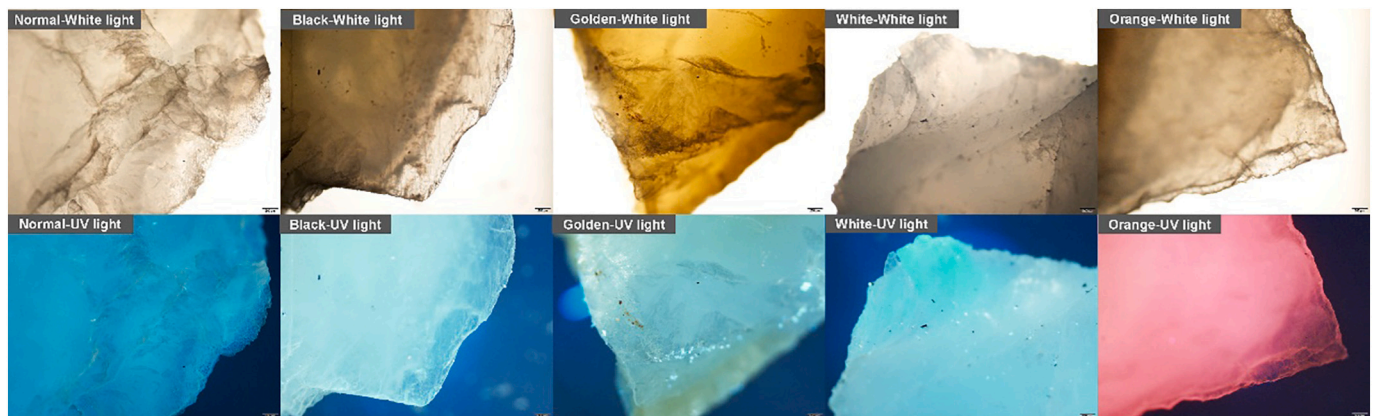
Fig. 3. Fluorescence microscope observation of the mantles of different color shell strains of *C.gigas* under white light and UV light. Noted that the red florescent was found in black-shell, white-shell, and orange-shell strains. (For interpretation of the references to color in this figure legend, the reader is referred to the web version of this article.)

biosynthetic pathway include the insertion of ferrous iron into proto-porphyrin IX by ferrochelatase, likely occurred in the mitochondria (Braz et al., 2001). The deduced amino acid sequences and domain of ALAS, ALAD, PBGD, UROS and UROD were shown in Supplementary Fig. S4, S6, S8, S10 and S12. The overall predicted haem pathway in *C. gigas* is shown in Fig. 6.

3.3. Homology and phylogenetic analysis of key haem pathway genes

The protein sequence similarities of ALAS, ALAD, PBGD, UROS and UROD among different species were displayed in Supplementary Table S9. Sequence alignment of *CgALAS* and *CgUROD* showed a moderate degree of sequence similarity. *CgALAD* and *CgUROS* displayed extremely high similarity among various species. As for *CgPBGD*, it had lower identity with *C. virginica* at 49.73% in the *Crassostrea* species.

The construction of phylogenetic tree allowed determination of evolutionary similarity among molluscs, teleost, amphibians, and mammals. As shown in Supplementary Fig. S5, vertebrates have both ALAS1 and ALAS2 genes, but invertebrates only have one ALAS. ALAS1 and ALAS2 from vertebrates were grouped together, and the invertebrate species were clustered with themselves. The vertebrates were clustered together and formed several branches including mammals, amphibians, and teleost. The invertebrates were clustered together and divided into four subgroups including bivalvia, arthropod, echinoderm

Fig. 4. Fluorescence microscope observation of the mantles of the orange-shell strain of *C. gigas* under white light and UV light. Noted that the red fluorescence of porphyrin pigment was observed in the outer calcification epithelium of the mantle margin of the orange-shell strain. (For interpretation of the references to color in this figure legend, the reader is referred to the web version of this article.)
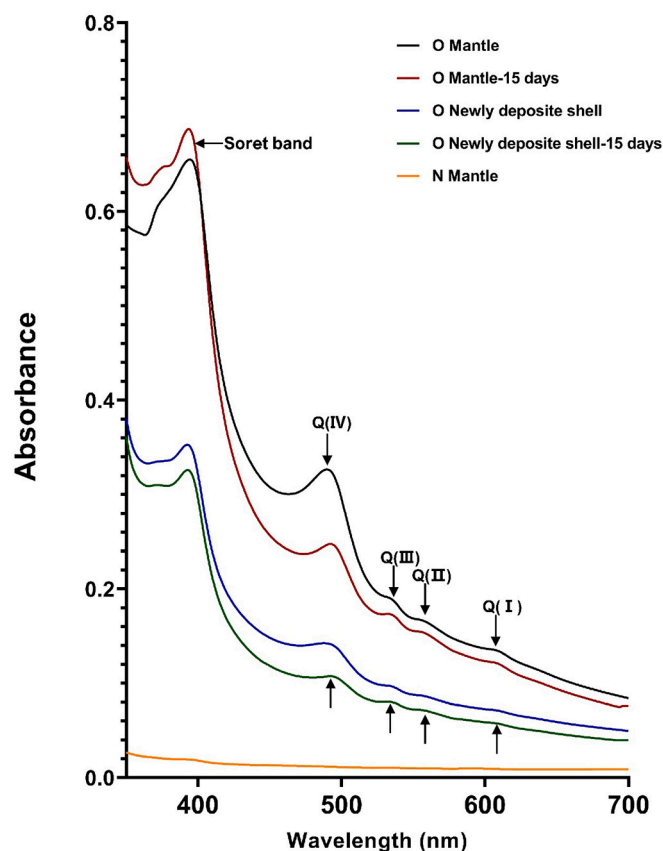
Fig. 5. UV–visible absorption spectra of the Na-EDTA aqueous extracts from the mantle, and newly deposited shell of orange-shell strain of *C. gigas* collected right after extraction and 15 days after extraction, together with the UV–visible absorption spectra of the normal-shell strain of *C. gigas* mantle. Positions of λ_{max} (Soret band) and Q bands Q(I)–Q(IV) are marked. N represents the normal-shell strain and O represents the orange-shell strain.

Table 2
Sequence features of *CgALAS, CgALAD, CgPBGD, CgUROS, CgUROD* from *C. gigas.*

	CgALAS	*CgALAD*	*CgPBGD*	*CgUROS*	*CgUROD*
Total length (bp)	20,673	6191	6583	16,622	3832
cDNA length (bp)	3928	2062	1462	2431	1431
ORF length (bp)	1848	990	1095	771	1110
5′UTR length (bp)	218	94	95	404	140
3′UTR length (bp)	1862	978	272	1244	181
Amino acids	615	329	364	267	369
Theoretical PI	5.92	7.55	5.96	5.24	4.89
Weight (kDa)	66.92	35.83	39.61	28.2	40.93
Number of exons	13	7	11	9	10
Number of introns	12	6	10	8	9
Positive (Arg + Lys)	56	33	41	22	28
Negative (Asp + Glu)	71	32	47	29	44

and platyhelminth. The maximum likelihood phylogenetic trees were built using ALAD, UROS and UROD amino acid sequences from various species. The phylogenetic analysis showed that invertebrates were clustered together and the *Crassostrea* species were closely related to *M. yessoensis* (Supplementary Fig. S7, S11 and S13). According to the maximum-likelihood tree of *CgPBGD* (Supplementary Fig. S9), all mollusc species were clustered together with *C. gigas* and *C. virginca* as a branch. Overall, the results of phylogenetic analysis were consistent with the traditional taxonomy.

3.4. Localization of mRNA expression and quantification of gene expression levels

The patterns of mRNA expression were determined for key genes in the haem pathway through *in situ* hybridization. The result revealed that *CgALAS, CgALAD, CgPBGD, CgUROS,* and *CgUROD* were expressed at the outer fold of *C. gigas* mantles (Fig. 7). Quantitative real-time PCR (qPCR) was used to estimate the gene expression levels encoding the first five enzymes in the haem pathway. Comparisons of relative levels of gene expression showed significant differences among strains. Values of *CgALAS* were significantly different between the five strains. The white-shell strain showed the highest level of expression. Lower expression was observed in the orange-shell strain and black-shell strain. As for golden-shell and normal-shell strain, a relatively low expression was discovered in mantle tissues (Fig. 8A). The expression level of *CgALAD* gene in orange-shell strain was significantly higher than other strains (Fig. 8B). Among the upstream and downstream genes which produced uroporphyrin I and III, the expression level of *CgPBGD* in orange-shell strain was significantly higher than that of other strains (Fig. 8C). Conversely, the *CgUROS* gene in orange-shell strain showed a significant lower expression level (Fig. 8D). As for the black-shell strain, the downstream gene *CgUROD* which degraded the uroporphyrinogen III was significantly higher than other strains ($p < 0.001$) (Fig. 8E). Probabilities for two-tailed paired t-tests of differences in gene regulation among strains of *C. gigas* could be found at Supplementary Table S6.

3.5. The expressions of CgALAS and CgPBGD protein in different shell-color strains

Western blotting was used to confirm the presence of key proteins in the haem pathway in *C. gigas* mantles, namely *CgALAS* and the *CgPBGD* with β-actin used as the control (Fig. 8F). The ALAS protein was chosen because of its initial position of the haem pathway and known to be the rate-controlling step of the heme biosynthesis in mammalian cells (Hunter and Ferreira, 2009). PBGD is the rate-limiting enzyme of the yeast haem production which may impact the accumulation of uroporphyrinogen I (Hoffman et al., 2003). The result confirmed *CgALAS* and *CgPBGD* protein expression in every tested mantles of Pacific oyster. Bands of *CgALAS* existed around 65 KDa which were consistent with the predicted molecular weight of 66.92 KDa. At the same time, the bands of *CgPBGD* appeared at the position of 40 KDa, which fits well with the predicted molecular weight of 39.61 KDa. Through the gray-scale quantifying, *CgALAS* appeared to be expressed more in the white-shell strain than others. The *CgPBGD* showed a higher expression in the mantle of the orange-shell strain. The specific gray-scale value could be found in Supplementary Table S7 and S8.

4. Discussion

The formation of shell colors is believed to be accomplished by a periodic and repetitive deposition of pigments produced by secretory cells of the mantle edge epithelium (Budd et al., 2014). Outer fold of the mantle contributes to shell formation (Parvizi et al., 2017). The dorsal mantle epithelium secretes mollusc shell and controls pigmentation (Boettiger et al., 2009; Budd et al., 2014). In this study, the auto-fluorescence of porphyrins under UV light was not only observed on the newly deposit shell and nacre of the orange-shell strain, but also at the outer fold of mantle. *In situ* hybridization revealed the expression of haem pathway genes at the outer fold of *C. gigas* mantle. This is consistent with the assumption that mantle edge accumulation and secretion of uroporphyrin I and III distributed the pigments in mantles of orange-shell strain *C. gigas*.

In this study, red florescence was also observed in the mantle of the black-shell strain. However, there was no red florescence found in the outer shell of black-shell strain, and the extraction of EDTA showed no characteristic peak of porphyrins. It has been suggested that purple and
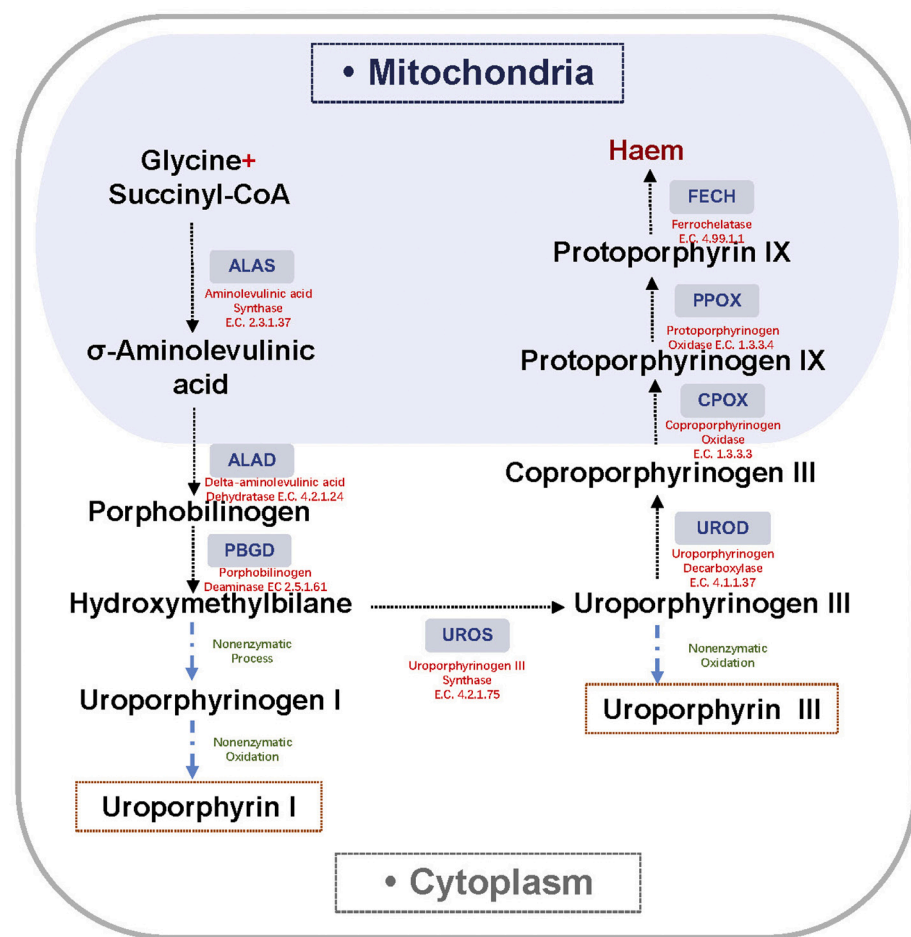
Fig. 6. Haem synthetic pathway in *C. gigas*. The eight enzymatic reactions which take place in mitochondria and cytoplasm produce haem and the nonenzymatic side paths resulting in the synthesis of uroporphyrin I and uroporphyrin III pigments (marked with a red dotted box). Light blue arrows indicate nonenzymatic processes. Enzyme names are in red font, metabolite names are in black font. Enzyme Commission (EC) numbers provide a numerical classification scheme for enzymes, based on the chemical reactions they catalyze. (For interpretation of the references to color in this figure legend, the reader is referred to the web version of this article.)

dark patterns of *C. gigas* shell are composed of uroporphyrin and its derivatives (Bonnard et al., 2020), black shell coloration in *P. margaritifera* was also due to porphyrins (Miyoshi et al., 1987). Though porphyrins are responsible for the dominant colors of pink-red and yellow-brown (Williams et al., 2017), black pigmentation was identified as a foreground color (Ge et al., 2015), the quenching ability of the melanin might cause the absence of red florescence (Comfort, 1951). It could be assumed that uroporphyrin I or III could not dominant the shell coloration when melanin exists.

The dominant shell pigments in *C. margaritarius* and *C. pharaonius* were determined to be uroporphyrin I and uroporphyrin III (Williams et al., 2016), and uroporphyrin had also been revealed to be composed to *C. gigas* shell colors (Bonnard et al., 2020). In this study, the first five haem pathway genes which are related to the synthesis of uroporphyrin I and uroporphyrin III in *C. gigas* were cloned. A single copy of the ALAS gene was identified in *C. gigas* which contrasts to the identification of two ALAS genes, ALAS1 and ALAS2, in vertebrates except *Ciona intestinalis* and *Branchiostoma belcheri*. *CgALAS* protein contained Preseq_ALAS, and Beta_elim_lyase conserved domains, and was predicted to be localized in the mitochondrial matrix space, it suggests that the ALAS gene performs as the first step of the haem pathway in the mitochondria in *C. gigas*. As for the second gene in the haem pathway, the therapeutic function of ALAD has been examined comprehensively only in mammals (Gacond et al., 2007). The identification of the ALAD domain which catalyze the formation of porphobilinogen by the dimerization of two molecules of 5-aminolaevulinic acid (ALA). The PBGD gene is the third enzyme of the haem biosynthetic pathway (Bayliss, 1967). The identification of PBGD had been presented in mammals, such as rat and human (Grandchamp et al., 1984; Lannfelt et al., 1989). The

identification of Porphobil_deam domain and Porphobil_deamC domain in *CgPBGD* is in agreement with its role in producing hydroxymethylbilane and the accumulation of uroporphyrin I in *C. gigas*. The correlation between UROS and uroporphyrins accumulation has been defined in rats and humans while the characterization of the UROD had been identified in prokaryotes such as salmonella (Xu et al., 2003). In this study, the identification of the HEM4 domain and URO-D domain represents the potential to generate the process of uroporphyrin III formation and degradation of the uroporphyrinogen III (Raux et al., 2000).

It has been suggested that porphyrin in shell pigmentation is produced *de novo* by the animal through the haem pathway where uroporphyrin I and uroporphyrin III are produced as side products (Hendry and Jones, 1980; Williams et al., 2017). Their formation can be enhanced when the metabolites ALA, porphobilinogen, and HMB were overproduced (Hibino et al., 2013). At the same time, when activity of UROS is diminished, HMB spontaneously closes and forms uroporphyrinogen I (Phillips, 2019; Warner et al., 1992).Our data demonstrated that distinct levels of gene expression and uroporphyrin I and III accumulation correlated with shell color in these specific strains of *C. gigas*. By comparing among five strains of *C. gigas*, the orange-shell *C. gigas* has visible porphyrin pigments on mantle edge where the first enzyme in the haem pathway (*CgALAS*) was significantly upregulated and *CgUROS* and *CgUROD* were significantly downregulated. It is consistent with the data from the western blot analysis showing larger quantity of *CgALAS* protein in the orange-shell *C. gigas*. Similar result was discovered in the mantle of *C. margaritarius*, whose shell pigments are known to be rich in uroporphyrin I and uroporphyrin III. Similar results have also been found in the Yesso scallop, *M. yessoensis*, which
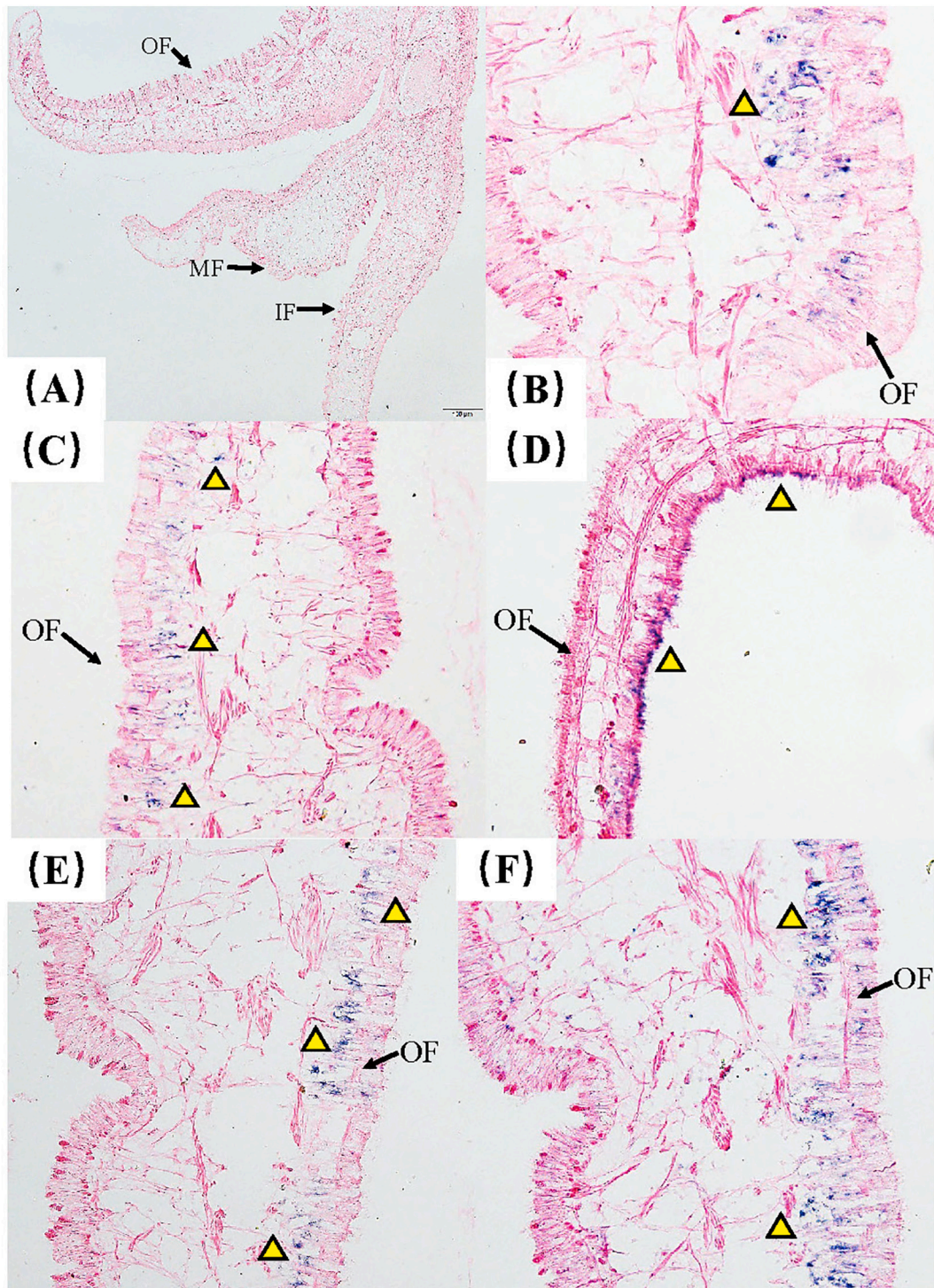
Fig. 7. Localization of *CgALAS*, *CgALAD*, *CgPBGD*, *CgUROS*, *CgUROD* gene expressions of *C. gigas* mantle by *in situ* hybridization. (A) RNA localization patterns of *CgALAS*, *CgALAD*, *CgPBGD*, *CgUROS*, *CgUROD* in *C. gigas* mantle. (B) Detection of the positive signal (blue/purple) of *CgALAS* in outer fold of *C.gigas* mantle. (C) Detection of the positive signal (blue/purple) of *CgALAD* in outer fold of *C.gigas* mantle.; (D) Detection of the positive signal (blue/purple) of *CgPBGD* in outer fold of *C.gigas* mantle; (E) Detection of the positive signal (blue/purple) of *CgUROS* in outer fold of *C.gigas* mantle; (F) Detection of the positive signal (blue/purple) of *CgUROD* in outer fold of *C.gigas* mantle. OF: outer fold of mantle; MF: middle fold of mantle; IF: inner fold of mantle. The positive signal (blue/purple) was marked by yellow triangles. (For interpretation of the references to color in this figure legend, the reader is referred to the web version of this article.)

showed significantly higher levels of expression of *PyALAS* in mantle tissue producing brown shells than mantle producing white shells (Mao et al., 2020). Furthermore, increasing levels of ALAS gene expression, and decreasing levels of UROS and UROD expression could simultaneously increase the production of uroporphyrin (To-Figueras et al., 2011). At the same time, increased expression of *CgPBGD* was found in

the orange-shell strain, and the highest quantity of *CgPBGD* protein was also discovered in the orange-shell strain. It has been suggested that the rising activity of this gene is known to be associated with uroporphyrin I production (Siersema et al., 1990). In this case, the upregulation of *CgALAS* and *CgPBGD* as well as the lower expression of *CgUROS* and *CgUROD* were indicative of more uroporphyrin I and III accumulation in
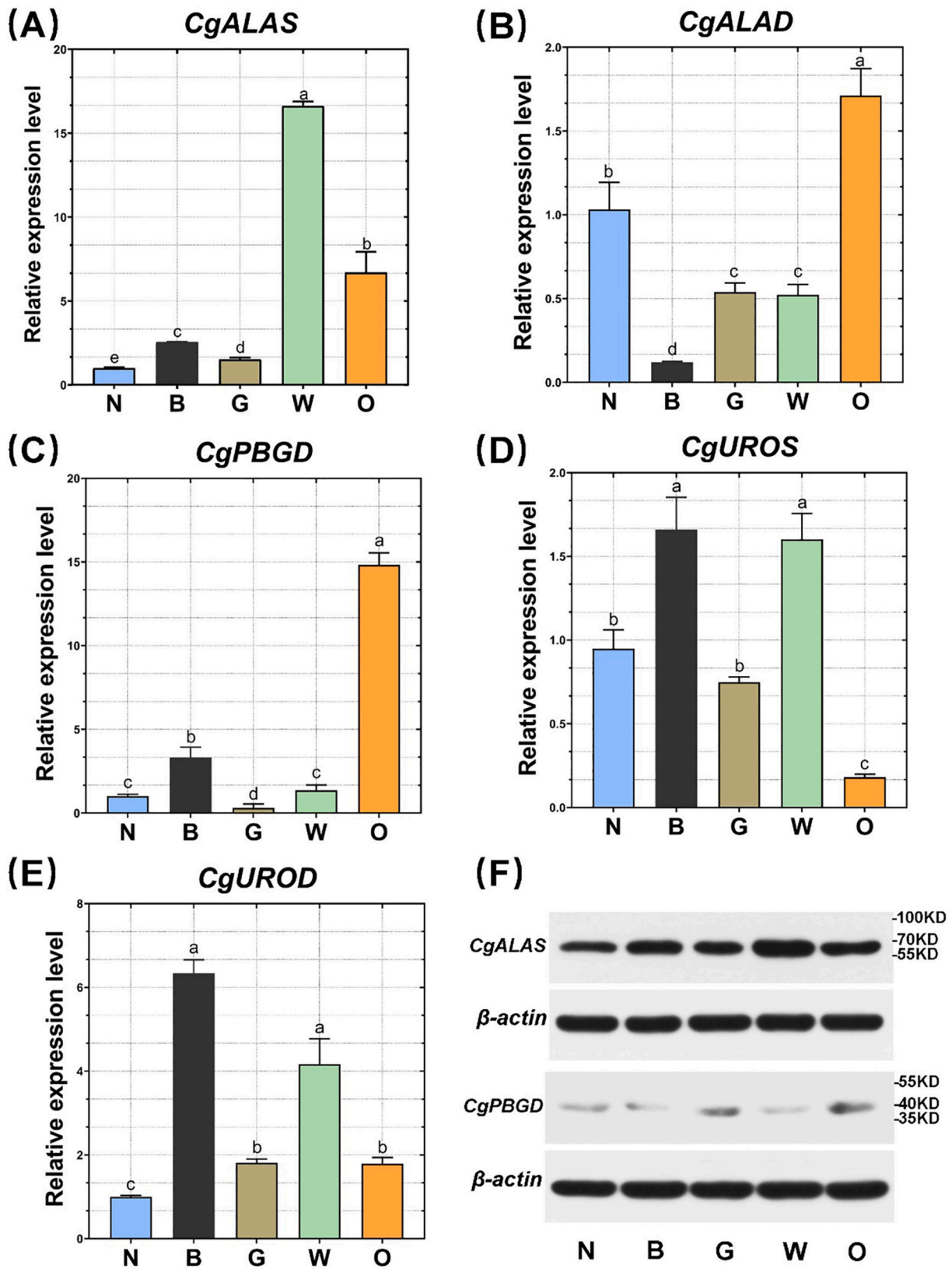
Fig. 8. Relative expression levels for the first five genes (*CgALAS*, *CgALAD*, *CgPBGD*, *CgUROS*, *CgUROD*) in the heme synthesis pathway compared between different color strains ($p < 0.05$) and western blot analysis of *CgALAS* and *CgPBGD* protein. (A-E) Relative expression levels of *CgALAS*, *CgALAD*, *CgPBGD*, *CgUROS*, *CgUROD* of *C. gigas* with different shell colors. Normalized expression was calculated relative to expression of Ef-α and comparisons were made among mantles of the N: normal-shell, B: black-shell, G: golden-shell, W: white-shell and O: orange-shell strains. Vertical bars represent the mean ± standard error (N = 3). Different letters indicate a significant difference ($p \leq 0.05$). (F) Western blot analysis: *CgALAS* and *CgPBGD* protein content were detected by western blotting in N: normal-shell, B: black-shell, G: golden-shell, W: white-shell and O: orange-shell strains. Each band represents the protein content of an individual, with the upper band representing the content of the *CgALAS* and *CgPBGD* protein and the lower band representing the content of *β-Actin*.

orange-shell strain than any other strains. Therefore, the activities of the haem pathway genes on *C. gigas* mantle could affect shell coloration by the metabolism of specific porphyrin pigments.

As for white-shell strain, the *CgALAS*, *CgUROS* and *CgUROD* gene expression was upregulated, lead to the decomposition of HMB and uroporphyrinogen III. Then the nonenzymatic reaction which leads to the production of uroporphyrin I and III are failed to be generated. As the whole white-shell strain shows no coloration on its outer shell, indicating the accumulation of trace amounts of uroporphyrin I and III or the absence of pigment, which is consistent with the results of the study. Comparable results were observed in the black-shell strain, the *CgPBGD* and *CgUROD* turned out to have high levels of expression at the same time, so there might be a decompose of uroporphyrinogen III. On contrary, the golden-shell strain showed lower expression of *CgALAS*, *CgALAD* and *CgPBGD*. Similarly, significantly higher levels of ALAD also occurred in mantle tissue of *C. zizyphinum* which does not produce porphyrins. It could indicate a less accumulation of uroporphyrinogen caused the absence of none-enzyme uroporphyrin I and III production process. Therefore, uroporphyrins in golden-shell strain of *C. gigas* were undetectable. Since the uroporphyrin contributed to shell color (Williams et al., 2016), and the significant differences of gene expression could lead to the presence and absence of uroporphyrins, suggesting that the shell color formation of *C. gigas* might be affected by the synthesis of these pigments.

Overall, the results obtained in this study demonstrate that uroporphyrin I and III pigments play an essential role in shell color formation of *C. gigas*. Several key genes in the haem pathway encode enzymes with conserved functional domains that could modulate the accumulation and degradation of specific types of uroporphyrinogen and affect the production of the by-product uroporphyrin I and III were identified. Comparison of porphyrin distribution and relative gene expression levels among five shell color strains of *C. gigas* support the important role of uroporphyrin I and III related haem pathway genes in shell coloration. Together, the present study provides new insights into the molecular mechanism of shell coloration in molluscs. Yet the regulatory mechanism of the porphyrin pigmentation in molluscs shell is not clear and remains to be explored.

Conflict of interest statement

We declare that we have no financial and personal relationships with other people or organizations that can inappropriately influence our work, there is no professional or other personal interest of any nature or kind in any product, service or company that could be construed as influencing the position presented in, or the review of, the manuscript entitled, " Identification and characterization of key haem pathway genes associated with the synthesis of porphyrin in the Pacific oyster (*Crassostrea gigas*)".

Acknowledgements

Appendix A. Supplementary data

Supplementary data to this article can be found online at https://doi.org/10.1016/j.cbpb.2021.110595.

References

Ajioka, R.S., Phillips, J.D., Kushner, J.P., 2006. Biosynthesis of heme in mammals. Biochim. Biophys. Acta (BBA) Mol. Cell Res. 1763, 723–736.

Bai, Z., Zheng, H., Lin, J., Wang, G., Li, G., 2013. Comparative analysis of the transcriptome in tissues secreting purple and white nacre in the pearl mussel *Hyriopsis cumingii*. PLoS One 8, e53617.

Bayliss, R.I.S., 1967. The metabolic basis of inherited disease. Am. J. Hum. Genet. 58, 600–601.

Boettiger, A., Ermentrout, B., Oster, G., 2009. The neural origins of shell structure and pattern in aquatic mollusks. Proc. Natl. Acad. Sci. U. S. A. 106, 6837–6842.

Bonnard, M., Cantel, S., Boury, B., Parrot, I., 2020. Chemical evidence of rare porphyrins in purple shells of *Crassostrea gigas* oyster. Sci. Rep. 10, 12150.

Braasch, I., Schartl, M., Volff, J.N., 2007. Evolution of pigment synthesis pathways by gene and genome duplication in fish. BMC Evol. Biol. 7, 74.

Braz, G.R.C., Abreu, L., Masuda, H., Oliveira, P.L., 2001. Heme biosynthesis and oogenesis in the blood-sucking bug, *Rhodnius prolixus*. Insect Biochem. Mol. Biol. 31, 359–364.

Budd, A., McDougall, C., Green, K., Degnan, B.M., 2014. Control of shell pigmentation by secretory tubules in the abalone mantle. Front. Zool. 11, 62.

Comfort, A., 1949. Acid-Soluble pigments of shells. 1. The distribution of porphyrin fluorescence in molluscan shells. Biochem. J. 44, 111–117.

Comfort, A., 1950a. Acid-soluble pigments of molluscan shells. 5. Identity of some subsidiary fractions derived from *Pinctada vulgaris*. Biochem. J. 47, 254–255.

Comfort, A., 1950b. Biochemistry of molluscan shell pigments. J. Molluscan Stud. 28, 79–85.

Comfort, A., 1950c. Molluscan shells as a practical source of uroporphyrin-I. Science 112, 279–280.

Comfort, A., 1950d. A subsidiary shell pigment of *Haliotis cracherodii* Leach. Nature 166, 194–195.

Comfort, A., 1951. The pigmentation of molluscan shells. Biol. Rev. 26, 285–301.

Cuthill, I.C., Allen, W.L., Arbuckle, K., Caspers, B., Chaplin, G., Hauber, M.E., Hill, G.E., Jablonski, N.G., Jiggins, C.D., Kelber, A., Mappes, J., Marshall, J., Merrill, R., Osorio, D., Prum, R., Roberts, N.W., Roulin, A., Rowland, H.M., Sherratt, T.N., Skelhorn, J., Speed, M.P., Stevens, M., Stoddard, M.C., Stuart-Fox, D., Talas, L., Tibbetts, E., Caro, T., 2017. The biology of color. Science 357, eaan0221.

Ding, J., Zhao, L., Chang, Y., Zhao, W.M., Du, Z., Hao, Z., 2015. Transcriptome sequencing and characterization of Japanese Scallop *Patinopecten yessoensis* from different shell color lines. PLoS One 10, e0116406.

Dixon, D.W., 2000. The colors of life: an introduction to the chemistry of porphyrins and related compounds. Q. Rev. Biol. 75, 45–46.

Dos Reis, I.M.M., Mattos, J.J., Garcez, R.C., Zacchi, F.L., Miguelao, T., Flores-Nunes, F., Toledo-Silva, G., Sasaki, S.T., Taniguchi, S., Bicego, M.C., Cargnin-Ferreira, E., Bainy, A.C.D., 2015. Histological responses and localization of the cytochrome P450 (CYP2AU1) in *Crassostrea brasiliana* exposed to phenanthrene. Aquat. Toxicol. 169, 79–89.

Elder, G.H., Roberts, A., 1995. Uroporphyrinogen decarboxylase. J. Bioenerg. Biomembr. 27, 207–214.

Feng, D., Li, Q., Yu, H., Zhao, X., Kong, L., 2015. Comparative transcriptome analysis of the Pacific Oyster *Crassostrea gigas* characterized by shell colors: identification of genetic bases potentially involved in pigmentation. PLoS One 10, e0145257.

Feng, D., Li, Q., Yu, H., Kong, L., Du, S., 2017. Identification of conserved proteins from diverse shell matrix proteome in *Crassostrea gigas*: characterization of genetic bases regulating shell formation. Sci. Rep. 7, 45754.

Feng, D., Li, Q., Yu, H., Kong, L., Du, S., 2018. Transcriptional profiling of long non-coding RNAs in mantle of *Crassostrea gigas* and their association with shell pigmentation. Sci. Rep. 8, 1436.

Frederic, M., Roy, N.L., Marie, B., 2012. The formation and mineralization of mollusk shell. Front. Biosci. 4, 1099–1125.

Gacond, S., Frère, F., Nentwich, M., Faurite, J.P., Frankenberg-Dinkel, N., Neier, R., 2007. Synthesis of bisubstrate inhibitors of porphobilinogen synthase from *Pseudomonas aeruginosa*. Chem. Biodivers. 4, 189–202.

Ge, J., Li, Q., Yu, H., Kong, L., 2015. Mendelian inheritance of golden shell color in the Pacific oyster *Crassostrea gigas*. Aquaculture 441, 21–24.

Grandchamp, B., Romeo, P.H., Dubart, A., Raich, N., Rosa, J., Nordmann, Y., Goossens, M., 1984. Molecular cloning of a cDNA sequence complementary to porphobilinogen deaminase mRNA from rat. Proc. Natl. Acad. Sci. U. S. A. 81, 5036.

Grotewold, E., 2006. The genetics and biochemistry of floral pigments. Annu. Rev. Plant Biol. 57, 761–780.

Hendry, G.A.F., Jones, O.T.G., 1980. Hemes and chlorophylls – comparison of function and formation. J. Med. Genet. 17, 1–14.

Hibino, A., Petri, R., Buechs, J., Ohtake, H., 2013. Production of uroporphyrinogen III, which is the common precursor of all tetrapyrrole cofactors, from 5-aminolevulinic acid by *Escherichia coli* expressing thermostable enzymes. Appl. Microbiol. Biotechnol. 97, 7337–7344.

Hoffman, M., Gora, M., Rytka, J., 2003. Identification of rate-limiting steps in yeast heme biosynthesis. Biochem. Biophys. Res. Commun. 310, 1247–1253.

Hu, Z., Song, H., Yang, M., Yu, Z., Zhou, C., Wang, X., Zhang, T., 2019. Transcriptome analysis of shell color-related genes in the hard clam *Mercenaria mercenaria*. Comp. Biochem. Physiol. D Genomics Proteomics 31, 100598.

Hunter, G.A., Ferreira, G.C., 2009. 5-aminolevulinate synthase: catalysis of the first step of heme biosynthesis. Cell. Mol. Biol. (Noisy le Grand) 55, 102–110.

Joron, M., Papa, R., Beltran, M., Chamberlain, N., Mavarez, J., Baxter, S., Abanto, M., Bermingham, E., Humphray, S.J., Rogers, J., Beasley, H., Barlow, K., ffrench-Constant, R.H., Mallet, J., McMillan, W.O., Jiggins, C.D., 2006. A conserved supergene locus controls color pattern diversity in *Heliconius* butterflies. PLoS Biol. 4, 1831–1840.

Kocot, K.M., Aguilera, F., McDougall, C., Jackson, D.J., Degnan, B.M., 2016. Sea shell diversity and rapidly evolving secretomes: insights into the evolution of biomineralization. Front. Zool. 13, 23.

Lannfelt, L., Wetterberg, L., Lilius, L., Thunell, S., Jörnvall, H., Pavlu, B., Wielburski, A., Gellerfors, P., 1989. Porphobilinogen deaminase in human erythrocytes: purification of two forms with apparent molecular weights of 40 kDa and 42 kDa. Scand. J. Clin. Lab. Invest. 49, 677–684.

Lemer, S., Saulnier, D., Gueguen, Y., Planes, S., 2015. Identification of genes associated with shell color in the black-lipped pearl oyster, *Pinctada margaritifera*. BMC Genomics 16, 568.

Livak, K.J., Schmittgen, T.D., 2001. Analysis of relative gene expression data using real-time quantitative PCR and the $2^{-\Delta\Delta CT}$ method. Methods 25, 402–408.

Mann, K., Jackson, D.J., 2014. Characterization of the pigmented shell-forming proteome of the common grove snail *Cepaea nemoralis*. BMC Genomics 15, 249.

Mao, J., Zhang, Q., Yuan, C., Zhang, W., Hu, L., Wang, X., Liu, M., Han, B., Ding, J., Chang, Y., 2020. Genome-wide identification, characterization and expression analysis of the ALAS gene in the Yesso scallop (*Patinopecten yessoensis*) with different shell colors. Gene 757, 144925.

McDougall, C., Degnan, B.M., 2018. The evolution of mollusc shells. Wiley Interdiscip. Rev. Dev. Biol. Biol. 7, e313.

Miyoshi, T., Matsuda, Y., Komatsu, H., 1987. Fluorescence from pearls and shells of black lip oyster, *Pinctada margaritifera*, and its contribution to the distinction of mother oysters used in pearl culture. Jpn. J. Appl. Phys. 26, 1069–1072.

Negro, J.J., Bortolotti, G.R., Mateo, R., Garcia, I.M., 2009. Porphyrins and pheomelanins contribute to the reddish juvenal plumage of black-shouldered kites. Comp. Biochem. Physiol. B 153, 296–299.

Nicholas, R.E.H., Comfort, A., 1949. Acid-soluble pigments of molluscan shells. 4. Identification of shell porphyrins with particular reference to conchoporphyrin. Biochem. J. 45, 208–210.

Parvizi, F., Monsefi, M., Noori, A., Ranjbar, M.S., 2017. Mantle histology and histochemistry of three pearl oysters: *Pinctada persica, Pinctada radiata* and *Pteria penguin*. Molluscan Res. 38, 11–20.

Phillips, J.D., 2019. Heme biosynthesis and the porphyrias. Mol. Genet. Metab. 128, 164–177.

Raux, E., Schubert, H.L., Warren, M.J., 2000. Biosynthesis of cobalamin (vitamin B12): a bacterial conundrum. Cell. Mol. Life Sci. 57, 1880–1893.

Robert, X., Gouet, P., 2014. Deciphering key features in protein structures with the new ENDscript server. Nucl. Acids Res. 42, 320–324.

Siersema, P.D., Derooij, F.W.M., Edixhovenbosdijk, A., Wilson, J.H.P., 1990. Erythrocyte porphobilinogen deaminase activity in porphyria-cutanea-tarda. Clin. Chem. 36, 1779–1783.

Taylor, J.D., Kennedy, W.J., Hall, A., 1969. The shell structure and mineralogy of the Bivalvia. Introduction. *Nuculacea trigonacea*. Bull. Br. Mus. Nat. Hist. Zool. Suppl. 3, 1–125.

To-Figueras, J., Ducamp, S., Clayton, J., Badenas, C., Delaby, C., Ged, C., Lyoumi, S., Gouya, L., de Verneuil, H., Beaumont, C., Ferreira, G.C., Deybach, J.C., Herrero, C., Puy, H., 2011. ALAS2 acts as a modifier gene in patients with congenital erythropoietic porphyria. Blood 118, 1443–1451.

Warner, C.A., Yoo, H.W., Roberts, A.G., Desnick, R.J., 1992. Congenital erythropoietic porphyria: identification and expression of exonic mutations in the uroporphyrinogen III synthase gene. J. Clin. Investig. 89, 693–700.

Wijesekera, T.P., Dolphin, D., 1985. Some preparations and properties of porphyrins. Adv. Exp. Med. Biol. 193, 229–266.

Williams, S.T., 2017. Molluscan shell colour. Biol. Rev. 92, 1039–1058.

Williams, S.T., Ito, S., Wakamatsu, K., Goral, T., Edwards, N.P., Wogelius, R.A., Henkel, T., de Oliveira, L.F., Maia, L.F., Strekopytov, S., Jeffries, T., Speiser, D.I., Marsden, J.T., 2016. Identification of shell colour pigments in marine snails *Clanculus pharaonius* and *C. margaritarius* (Trochoidea: Gastropoda). PLoS One 11, e0156664.

Williams, S.T., Lockyer, A.E., Dyal, P., Nakano, T., Churchill, C.K.C., Speiser, D.I., 2017. Colorful seashells: identification of haem pathway genes associated with the synthesis of porphyrin shell color in marine snails. Ecol. Evol. 7, 10379–10397.

With, T.K., 1978. On porphyrins in feathers of owls and bustards. Int. J. BioChemiPhysics 9, 893–895.

Wittkopp, P.J., Beldade, P., 2009. Development and evolution of insect pigmentation: genetic mechanisms and the potential consequences of pleiotropy. Semin. Cell Dev. Biol. 20, 65–71.

Xu, K., Ndivo, V., Majumdar, D., 2003. Cloning and expression of *Chlorobium vibrioforme* uroporphyrinogen decarboxylase gene in a salmonella heme auxotroph. Curr. Microbiol. 45, 456–458.

Xu, M., Huang, J., Shi, Y., Zhang, H., He, M., 2019. Comparative transcriptomic and proteomic analysis of yellow shell and black shell pearl oysters, *Pinctada fucata martensii*. BMC Genomics 20, 469.

Yu, H., Zhao, X., Li, Q., 2016. Genome-wide identification and characterization of long intergenic noncoding RNAs and their potential association with larval development in the pacific oyster. Sci. Rep. 6, 20796.